ORIGINAL ARTICLE

Morphometric Spatial Patterns Differentiating Boys With Fragile X Syndrome, Typically Developing Boys, and Developmentally Delayed Boys Aged 1 to 3 Years

Fumiko Hoeft, MD, PhD; Amy A. Lightbody, PhD; Heather Cody Hazlett, PhD; Swetapadma Patnaik, MS; Joseph Piven, MD; Allan L. Reiss, MD

Context: Brain maturation starts well before birth and occurs as a unified process with developmental interaction among different brain regions. Gene and environment play large roles in such a process. Studies of individuals with genetic disorders such as fragile X syndrome (FXS), which is a disorder caused by a single gene mutation resulting in abnormal dendritic and synaptic pruning, together with healthy individuals may provide valuable information.

Objective: To examine morphometric spatial patterns that differentiate between FXS and controls in early childhood.

Design: A cross-sectional in vivo neuroimaging study.

Setting: Academic medical centers.

Participants: A total of 101 children aged 1 to 3 years, comprising 51 boys with FXS, 32 typically developing boys, and 18 boys with idiopathic developmental delay.

Main Outcome Measures: Regional gray matter volume as measured by voxel-based morphometry and manual tracing, supplemented by permutation analyses; regression analyses between gray and white matter volumes, IQ, and fragile X mental retardation protein level; and linear support vector machine analyses to classify group membership.

Results: In addition to aberrant brain structures reported previously in older individuals with FXS, we found reduced gray matter volumes in regions such as the hypothalamus, insula, and medial and lateral prefrontal cortices. These findings are consistent with the cognitive and behavioral phenotypes of FXS. Further, multivariate pattern classification analyses discriminated FXS from typical development and developmental delay with more than 90% prediction accuracy. The spatial patterns that classified FXS from typical development and developmental delay included those that may have been difficult to identify previously using other methods. These included a medial to lateral gradient of increased and decreased regional brain volumes in the posterior vermis, amygdala, and hippocampus.

Conclusions: These findings are critical in understanding interplay among genes, environment, brain, and behavior. They signify the importance of examining detailed spatial patterns of healthy and perturbed brain development.

Arch Gen Psychiatry. 2008;65(9):1087-1097

Author Affiliations: Center for Interdisciplinary Brain Sciences Research, Stanford University School of Medicine, Stanford, California (Drs Hoeft, Lightbody, and Reiss and Ms Patnaik); and the Neurodevelopmental Disorders Research Center and Department of Psychiatry, University of North Carolina, Chapel Hill (Drs Hazlett and Piven).

HUMAN BRAIN MATURATION is a complex process that can now be examined in detail using in vivo neuroimaging techniques.[1] Early neuroimaging investigations focused on region, lobe, or total brain volumes.[1] However, more recent studies have begun to examine brain structures using finer voxelwise resolution and temporal dynamics. These new approaches have proven useful in advancing our understanding of associations between cognition and healthy brain development.[2]

Pediatric neuroimaging studies to date have primarily focused on healthy children aged 4 years and older using univariate approaches. However, brain maturation starts well before birth and occurs as a unified process with interregional interactions and dependencies. It is therefore critical to investigate spatial neurodevelopmental patterns using multivariate approaches in children soon after birth. It is also important to examine abnormal brain states to more fully understand normal brain maturational processes. Studies of fragile X syndrome (FXS) in early childhood may provide these unique opportunities.

Unlike many developmental disorders that are symptomatically defined and therefore likely to be heterogeneous, FXS has a well-characterized genetic etiology. It is an X-linked disorder caused by a mutation of the fragile X mental retardation-1 (*FMR1*) gene (GenBank L29074) leading to diminished production of the associated fragile X mental retardation protein (FMRP). In turn, the diminished FMRP level negatively affects synaptic maturation and plasticity and thus cerebral development.[3] The disorder results in impaired cognition and aberrant behavior, including deficits in executive and social function, learning and memory, visuospatial skills, and emotion regulation.[4]

As a component of an ongoing longitudinal study of brain development in FXS, we examined magnetic resonance images (MRIs) of 51 boys with FXS, 32 typically developing (TD) boys, and 18 boys with idiopathic developmental delay (DD) aged 1 to 3 years. The main goals of the study were to examine structural brain abnormalities in FXS compared with both TD and DD and to examine neurodevelopmental differences in these very young subjects with FXS relative to findings reported in older subjects with FXS.[4-7] Primary analytical methods included univariate between-group comparisons and multivariate pattern classification methods. We hypothesized that regions best distinguishing the young FXS group from control subjects, such as the caudate, would show associations with FMRP levels as well as with cognitive measures (IQ). Negative associations between FMRP levels and caudate volumes have been shown in youth and adults but not in children of this age range.[5,8] We further hypothesized that morphometric patterns would accurately classify participants into their respective groups.

METHODS

PARTICIPANTS

The study protocols were approved by the human subjects committees at Stanford University School of Medicine, Stanford, California, and University of North Carolina, Chapel Hill (UNC). Consent was obtained from parents. Subjects included 51 boys with FXS (mean [SD] age, 35.0 [7.6] months), 32 TD boys (mean [SD] age, 29.7 [7.1] months), and 18 boys with idiopathic DD (mean [SD] age, 34.8 [5.1] months). Five participants with FXS and 3 TD participants have been included in a previous article.[5]

Subjects in all of the groups were recruited by Stanford University and UNC. Recruitment of children with FXS was accomplished using both the Stanford University and UNC registry databases, frequent postings on the National Fragile X Foundation Web site and in the quarterly newsletter, and mailings to regional FXS organizations. Children with DD and TD were recruited locally through early intervention programs, preschools, child care centers, community media, and state-run agencies (Regional Center system in California and Child Development Service Agencies in North Carolina). Inclusion in the FXS group required DNA testing that confirmed the fragile X full mutation as diagnosed with the standard Southern blot technique. Participants in the DD group included children with DD of unknown etiology who did not exhibit symptoms indicative of an autism spectrum disorder. All of the children in this group demonstrated a composite standard score (SS) below 85 (<1 SD) on the Mullen Scales of Early Learning.[9] Exclusion criteria for all of the groups included preterm birth (<34 weeks' gestation), low birth weight (<2000 g), evidence of a genetic condition or syndrome, sensory impairments, and any serious medical or neurological condition affecting growth and development (eg, seizure disorder, diabetes, or congenital heart disease).

Testing of DNA for the typical *FMR1* expansion mutation was performed to confirm the presence of the full mutation in all of the subjects with FXS for whom the diagnostic status was uncertain and to rule out FXS in DD control subjects. Standard Southern blot was performed, followed by *FMR1*-specific probe hybridization.[10] Expression of FMRP was ascertained by calculating the percentage of peripheral lymphocytes containing FMRP using immunostaining techniques.[11]

Subjects were given a standard battery of measures including the Mullen Scales of Early Learning,[9] the Vineland Adaptive Behavior Scales,[12] the Child Behavior Checklist,[13] and the Repetitive Behavior Scales.[14,15] There was a significant difference in age between subjects with FXS and TD ($P=.001$) and between subjects with DD and TD ($P=.02$) but not between subjects with FXS and DD ($P=.91$). Vineland Adaptive Behavior Scales composite SSs were also significantly different between subjects with FXS and TD ($P<.001$) and between subjects with DD and TD ($P<.001$) but not between subjects with FXS and DD ($P=.33$). Mullen Scales of Early Learning composite SSs were significantly different between subjects with FXS and TD ($P<.001$) and between subjects with DD and TD ($P<.001$) but not between subjects with FXS and DD ($P=.38$). **Table 1** shows details of the 3 groups and between-group statistics.

Overall, 50 subjects were recruited at Stanford University and 51 were recruited at UNC. There were no significant differences between sites in the proportion of diagnoses ($\chi^2=1.51$; $P=.47$). For each diagnostic group, age ($P=.31$-$.73$), Vineland Adaptive Behavior Scales SSs ($P=.20$-$.94$), Mullen Scales of Early Learning SSs ($P=.43$-$.61$), and FMRP levels ($P=.62$, FXS only) did not differ between sites. Four individuals with FXS and 2 with DD were receiving medication (FXS: 1 was receiving bethanechol chloride, 1 was receiving piracetam, and 2 were receiving clonidine hydrochloride; DD: 1 was receiving memantine and 1 was receiving lamotrigine).

MRI PREPARATION AND ACQUISITION

All of the subjects with FXS or DD were sedated during their MRI. A pediatric anesthesiologist (Brenda Golianu, MD, Imad Yamout, MD, and Allison Ross, MD) administered and monitored the sedation throughout the scan. The TD children were scanned while sleeping. For the sleep scans, parents were instructed to wake their children a little earlier on the morning of the scan and to shorten their nap time. Scans were scheduled for after the participants' normal bedtime to ensure the children would be able to sleep during the scan. Parents received a packet of preparation materials for the scan that included a CD of scanner sounds to desensitize the children to the noise of the scanner while sleeping. Further, these subjects participated in a simulated MRI situation to practice holding still and to alleviate fear should the child awaken during the MRI.

General Electric 1.5-T Signa LX scanners (GE Healthcare, Milwaukee, Wisconsin) and standard transmit/receive 4-channel head coils were used for MRI acquisition. Scans were obtained from 2003 through 2007 and were performed at the Lucile Packard Children's Hospital, Stanford University and at the Brain Imaging and Analysis Center, UNC. Identical pulse sequence protocols were used at both scan sites, and they were designed to maximize contrast between gray matter (GM), white matter (WM), and cerebrospinal fluid for the participants' age

Table 1. Demographic Information

Characteristic	Mean (SD)			ANOVA	
	FXS (n=51)	TD (n=32)	DD (n=18)	*F* Score	*P* Value
Age, mo	35.0 (7.6)	29.7 (7.1)	34.8 (5.1)	6.16	.003
Mullen Scales of Early Learning composite standard score	54.65 (8.98)	108.50 (18.42)	57.72 (9.71)	187.04	<.001
Vineland Adaptive Behavior Scales composite standard score	62.02 (9.67)	97.23 (12.44)[a]	65.00 (11.92)	105.30	<.001
FMRP level, %	5.74 (3.41)[b]				

Abbreviations: ANOVA, analysis of variance; DD, developmentally delayed; FMRP, fragile X mental retardation protein; FXS, fragile X syndrome; TD, typically developing.

[a] The sample size was 31.

[b] The sample size was 46.

range. This included a coronal T1-weighted sequence with the following parameters: inversion recovery preparation pulse, 300 milliseconds; repetition time, 12 milliseconds; echo time, 5 milliseconds; flip angle, 20°; thickness, 1.5 mm; number of excitations, 1; field of view, 20 cm; and matrix, 256×192. An MRI quality control phantom (Data Systems, Inc, Hillsboro, North Carolina) was scanned after each subject at both sites to standardize assessments over sites, individuals, and time.

IMAGE PROCESSING

Voxel-Based Morphometry Analyses

Voxel-based morphometry (VBM) analyses of T1-weighted MRIs were performed using SPM5 (http://www.fil.ion.ucl.ac.uk/spm) and VBM5 (http://dbm.neuro.uni-jena.de/vbm) software. After bias correction, T1-weighted images were segmented to GM, WM, and cerebrospinal fluid. Hidden Markov random field (prior probability weight 0.3) was used to encode spatial information through spatial constraints of neighboring voxels. Normalization was performed using the following parameters: 12-parameter affine transformation and 3-dimensional discrete cosine transformation basis function (12×12×*, where * is calculated to yield a spatial cutoff that is 25 in all directions). Linear and nonlinear jacobian modulation was then applied (reflecting GM volume [GMV] and WM volume [WMV]), followed by smoothing with an isotropic gaussian kernel with full-width at half-maximum of 8 mm. Smoothing was also performed at 4 mm and the same regions were detected. For example, the FXS>TD, DD contrast showed caudate, thalamus, hypothalamus, fusiform gyrus, and occipital regions, and the TD, DD>FXS contrast showed superior temporal gyrus, hippocampus, insula, and orbitofrontal and medial prefrontal cortices at $P=.05$, familywise-error corrected. Customized GM and WM templates created from all of the subjects were used for VBM processing. Segmentation and normalization for each subject were confirmed by manual inspection of the images. Two DD participants were excluded from this study as a result of poor segmentation (final N=18).

Volumetric Measures

Left and right total caudate nuclei volumes were obtained with the automated segmentation of caudate nucleus algorithm[16] using BrainImageJava (http://cibsr.stanford.edu), a public-domain program for morphological image processing originally developed as a component of the National Institutes of Health Human Brain Project. The validity of the algorithm was tested with 55 high-resolution T1-weighted MRI data sets, and the segmentation results were overlaid onto the original image data for visual inspection. The algorithm was run on the registered and inhomogeneity-corrected images. The right and left caudate volumes for each subject were checked manually and were corrected if necessary.

The amygdala was manually traced on high-resolution T1-weighted images aligned along the long axis of the hippocampus using the IRIS/SNAP tool at UNC. The protocol developed by the Center for Neuroscience and the MIND Institute at the University of California, Davis was used[17] (see http://www.psychiatry.unc.edu/autismresearch/mri/ROIs/Amygdala.pdf for details). We first established reliability with the University of California, Davis group (average interrater reliability=0.92). Subsequently, reliability was established on scans from a sample of 18- to 35-month-old children. Reliability was obtained by 2 raters (Matthew Mosconi, PhD, and Michael Graves, MChe) who made independent measurements on a set of 15 images, which included 5 images repeated 3 times (in random order). Intrarater and interrater reliabilities (intraclass correlation) were 0.90 and 0.78, respectively. Two raters (who had the reliability of 0.90) performed all of the amygdala traces. There were 7 cases (4 with TD, 2 with DD, and 1 with FXS) that were of insufficient quality to obtain an amygdala trace.

The cerebellar vermis was manually delineated into the anterior vermis (I-V lobules), mid vermis (VI-VII lobules), and posterior vermis (VIII-X lobules) using BrainImage 3.7 software (http://cibsr.stanford.edu). The protocol required selecting the best midsagittal slice as defined by prioritizing clarity of the following structures: cerebellar vermis, cerebral aqueduct, corpus callosum, and brain stem. All of the analyses were performed independently by 2 raters (S.P. and Asya Kamrchemskiy, MS) who were blinded on the subjects' diagnosis and achieved interrater reliability of 0.95. The raters made 2 tracings of the 3 vermal regions for each subject and the values were averaged.

STATISTICAL ANALYSIS

Cross-Site Analysis

We undertook a number of procedures to ensure compatibility of MRIs across sites. First, we used the same pulse sequence and the same scanner type at each site. Second, to characterize scanner quality, we calculated the signal to noise ratio for 24 random phantom scans (12 per scanner, selected across the entire period of the study by an investigator blind to the scan site and date on which the data were collected [F.H.]) using the method described by Henkelman.[18] Two signal to noise ratio measurements were performed and were not significantly different across sites ($P=.39$ and $P=.22$). Third, we examined whether brain volumes differed as a function of scan site. The

Table 2. Gray Matter Regions That Show Significant Differences Between Fragile X Syndrome and Control Groups

ROI Name	Region	Brodmann Area	Talairach Coordinates x	y	z	*T* Value	*P* Value, FWE Corrected	Cluster Size
			FXS > TD, DD					
A	Right caudate body, head		14	2	19	10.28	< .001	7120
			14	19	−2	7.07	< .001	
B	Left caudate body, head		−17	4	20	9.11	< .001	6699
			−12	21	−1	7.29	< .001	
C	Left precentral, inferior frontal gyri	6	−44	−1	28	7.11	< .001	591
D	Right fusiform gyrus	18, 19	37	−76	−12	6.77	< .001	1857
			41	−86	−12	6.22	.001	
			31	−91	−15	6.20	.001	
E	Bilateral thalamus (dorsal medial, ventral anterior nuclei), hypothalamus		6	−10	13	6.71	< .001	1506
			−7	−11	13	6.61	< .001	
			−8	−14	5	6.39	< .001	
F	Left middle, superior occipital gyri	19	−43	−86	19	6.59	< .001	714
G	Right anterior cerebellum		26	−45	−24	6.37	< .001	322
H	Left cingulate gyrus	23	−5	−26	32	5.57	.01	235
			TD, DD > FXS					
a	Right insula	13	30	12	11	9.21	< .001	4951
			40	−4	19	8.22	< .001	
b	Left insula	13	−39	−3	19	9.17	< .001	3801
			−30	14	13	8.05	< .001	
c	Right hippocampal gyrus		33	−39	8	6.87	< .001	2514
			30	−57	17	5.55	.004	
d	Right postcentral gyrus, IPL	40, 1, 3	57	−27	20	6.74	< .001	5899
			58	−16	43	6.62	< .001	
			62	−7	16	6.41	< .001	
e	Right postcentral gyrus, IPL	40	49	−30	48	6.68	< .001	556
			62	−28	41	5.54	.01	
f	Right medial frontal gyrus	10	13	52	−6	6.48	< .001	484
g	Right inferior frontal gyrus	44, 45	53	17	18	6.44	<.001	1162
			59	9	19	5.95	.002	
h	Left middle frontal gyrus	11	−22	41	−13	6.34	< .001	431
i	Left medial frontal gyrus		−10	53	5	6.19	.001	1372
			−12	44	13	5.95	.002	
			−9	43	0	5.68	.006	
j	Left hippocampal gyrus		−33	−37	6	6.14	< .001	468
k	Left IPL, postcentral gyrus	40	−62	−34	38	6.09	.001	395
l	Right medial frontal gyrus	11	6	44	−14	5.96	.002	408
			15	39	−15	5.80	.004	
m	Left precentral gyrus	6, 4	−62	−4	27	5.87	.003	1083
			−61	−10	38	5.76	.005	
			−65	−19	42	5.15	.04	
n	Left superior temporal, precentral gyri	22, 4	−62	−8	3	5.59	.009	232
			−54	−8	5	5.39	.02	

Abbreviations: DD, developmentally delayed; FWE, familywise error; FXS, fragile X syndrome; IPL, inferior parietal lobule; ROI, region of interest; TD, typically developing.

GMV, WMV, cerebrospinal fluid volume, and total tissue volume (TTV) (GMV + WMV) were not significantly different across sites (all $P > .05$). Volumetric measurements of caudate nuclei, amygdala, and vermis did not differ significantly across scan sites ($P > .05$). All of the regions we describe later that showed significant differences in regional brain volumes between groups also did not show significant differences between scan sites except for the following regions: right cerebellar GMV (region G in **Table 2**) and precentral and postcentral GMV (regions C, d, and m in Table 2) and WMV (region a in **Table 3**). Fourth, we included scan site as a nuisance variable in all of the analyses that we report because of the small (nonsignificant) differences found between sites. Finally, we repeated the VBM analyses for each scan site separately. While this reduced the sample size to half, the only region that was no longer significant was a right anterior cerebellar GM region (region G in Table 2), and regions that showed only trends for significant differences were 2 of the 3 right medial frontal WM regions (regions c and i in Table 3).

Analyses of GMV, WMV, and Cerebrospinal Fluid Volume

We examined total GMV, WMV, and TTV obtained from VBM analyses using a univariate general linear model followed by post hoc analyses. Diagnostic group and scan site were included as fixed factors, and age was included as a covariate. Site × diagnosis interaction was not modeled as this factor was not significant ($P > .10$) for any comparisons performed. Further analyses were performed by including IQ (Mullen Scales of Early Learning composite SS) as a covariate.

Table 3. White Matter Regions That Show Significant Differences Between Fragile X Syndrome and Control Groups

ROI Name	Region	Talairach Coordinates x	y	z	*T* Value	*P* Value, FWE Corrected	Cluster Size
		FXS > TD, DD					
A	Right insular ventrolateral prefrontal region	31	8	14	8.38	< .001	1283
		33	−14	17	6.53	< .001	
B	Left insular ventrolateral prefrontal region	−30	12	13	8.20	< .001	
		−38	−3	20	7.30	< .001	1175
		−33	−14	19	6.88	< .001	
C	Left superior temporal region	−40	−51	23	7.07	< .001	1374
D	Right medial temporal region	39	−41	−5	6.60	< .001	1022
		34	−32	1	6.37	< .001	
E	Left medial temporal region	−37	−45	−6	6.10	< .001	723
F	Right middle occipital region	34	−67	3	5.74	.002	252
		TD, DD > FXS					
a	Left precentral ventrolateral prefrontal region	−45	−1	27	8.52	< .001	1762
b	Left caudate, medial frontal region	−14	20	−1	8.35	< .001	
		−20	16	13	7.53	< .001	2083
		−20	9	19	7.23	< .001	
c	Right caudate, medial frontal region	14	20	0	7.56	< .001	444
d	Right precentral ventrolateral prefrontal region	46	−3	27	6.95	< .001	2075
		36	−6	39	5.88	.001	
e	Left precentral and postcentral region	−30	−29	50	6.29	< .001	249
f	Right medial frontal region	24	39	11	6.06	.001	413
g	Left dorsolateral prefrontal region	−32	33	21	5.66	.003	248
h	Right postcentral, inferior parietal region	47	−18	29	5.64	.003	411
i	Right superior, medial frontal region	−21	40	19	5.49	.005	224
		−24	39	9	5.22	.01	

Abbreviations: DD, developmentally delayed; FWE, familywise error; FXS, fragile X syndrome; ROI, region of interest; TD, typically developing.

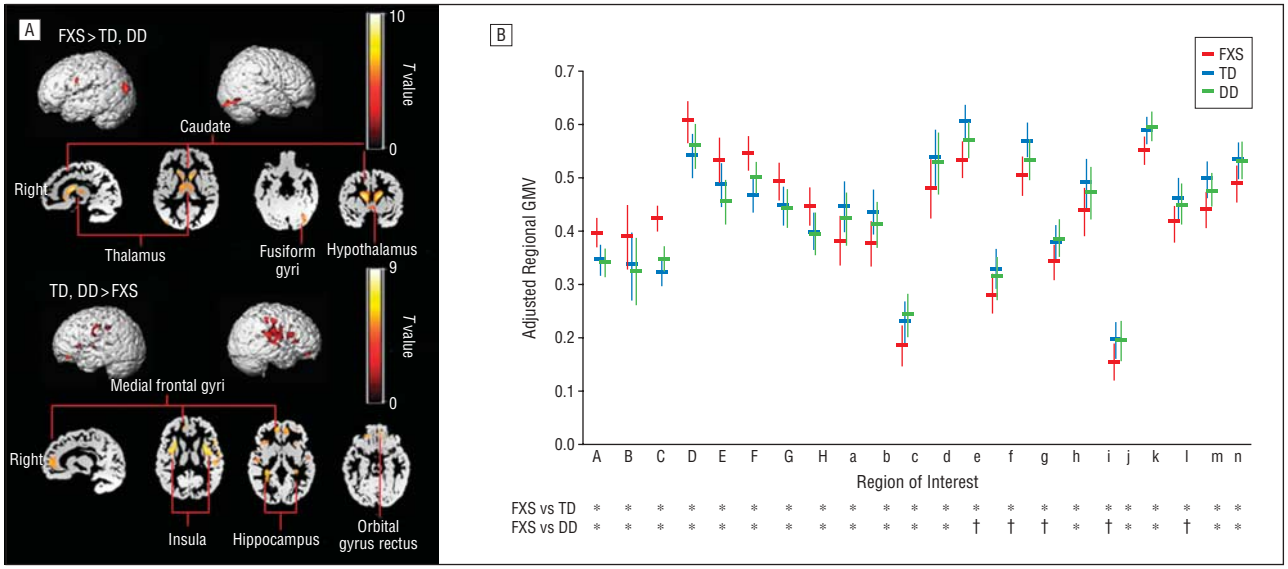

Figure 1. Differences in gray matter volume (GMV) between groups. A, Regions that show significant differences in GMV between fragile X syndrome (FXS) and controls. TD indicates typically developing; DD, developmentally delayed. $P = .05$, familywise-error corrected, extent threshold = 200. B, Adjusted GMVs are plotted to ensure that only 1 control group (TD or DD) is not driving the overall effect. Letters on the x-axis correspond to region of interest labels in Table 2. Error bars represent SD. *$P < .001$. †$P < .01$.

VBM Analysis

We examined regional GM and WM differences between FXS and controls using whole-brain analysis of covariance, covarying out age, scan site, and global and total GMV and WMV (for regional GM and WM analyses, respectively). For this analysis, we initially combined the TD and DD groups (n = 50) and compared with the FXS group (n = 51) to match sample sizes. We confirmed the results by performing a 1-way analysis of covariance (with the same covariates as described earlier) but by treating the participants with FXS, TD, and DD as 3 separate groups (this showed similar results). To ensure that the significant effects were not driven by one of the control groups, the following analyses were performed. First, mean values from signifi-

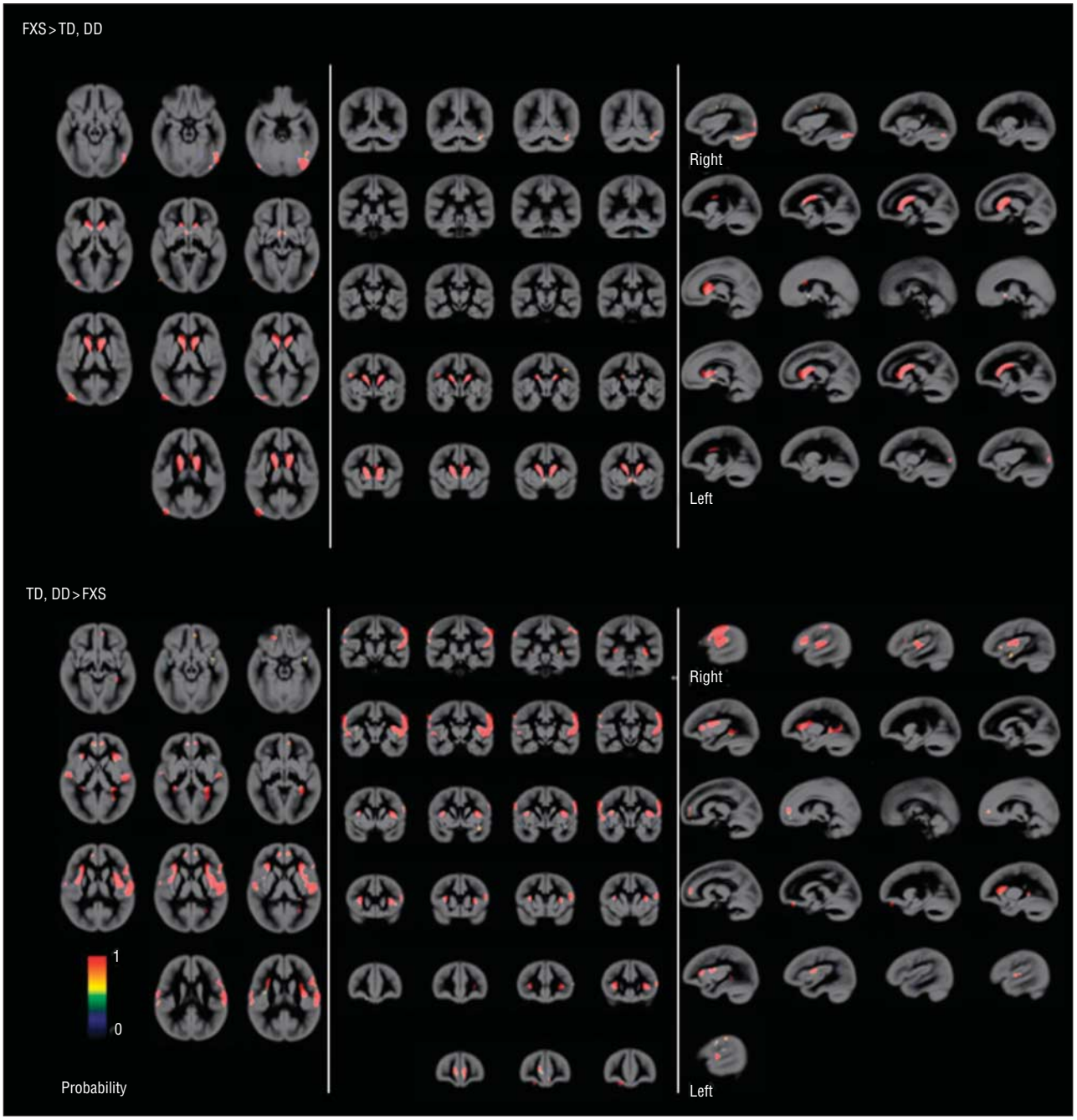

Figure 2. Probabilistic maps of regional gray matter volume differences between groups. Gray matter regions that show significantly greater and less volumes in fragile X syndrome (FXS) compared with typically developing (TD) and developmentally delayed (DD) groups were examined using leave-one-out cross-validation analysis permuted 102 times. Scaling bar indicates *T* values. A value of 1 in a given voxel indicates that all of the permutations showed significant effects (at a threshold of $P = .05$, familywise-error corrected, extent threshold = 200). Age, scan site, and total gray matter volume were entered as nuisance variables. Statistical maps are overlaid on a custom gray matter template. Most regions showing a value of 1 indicate the consistency of results. The left hemisphere is shown on the left side.

cant brain regions in the whole-brain VBM analyses described earlier were extracted for each subject. These values were then adjusted for age, scan site, and total GMV and WMV for GM and WM analyses, respectively. Values were adjusted by performing linear multiple regression analysis with age, scan site, and total GMV and WMV as independent variables and then obtaining the residuals. These adjusted brain volumes were compared between FXS and TD and between FXS and DD separately.

A statistical threshold of $P = .05$, familywise-error corrected, with an extent threshold of 200 was used, correcting for nonisotropic smoothness. Statistical images were overlaid onto normalized GM and WM images from a representative subject with TD, DD, or FXS. Brain regions with significant effects are reported based on their anatomical locations overlaid on the custom template and several sample FXS, TD, and DD T1-weighted images from this study. Although it is not necessarily valid to report Talairach coordinates and Brodmann areas because of the very young study sample and the use of custom templates, we report these as a reference for comparisons with other studies. The reported Talairach coordinates were converted from MNI space using the mni2tal function (http://www.mrc-cbu.cam.ac.uk/Imaging/Common/mnispace.shtml), and

Brodmann areas were identified using Talairach Daemon (Research Imaging Center, University of Texas Health Science Center, San Antonio). These Brodmann areas and labels were confirmed with the Talairach atlas.[19]

To examine the consistency of the results, probabilistic GM maps of the VBM results were constructed by performing leave-one-out permutation analysis. The aforementioned between-group VBM GM analysis was repeated 100 times leaving 1 subject out at a time. The statistical images were thresholded similarly, binarized, and summed to create probabilistic maps. The results were overlaid on a custom GM template.

Volumetric Analysis of Caudate Nuclei, Amygdala, and Vermis

We examined volumes of left and right caudate nuclei, left and right amygdala, and anterior, middle, and posterior vermis adjusting for age, scan site, and TTV or total GMV (for total and GM caudate volumes, respectively) using the same method as described earlier for GMV, WMV, and TTV comparisons. The only difference was that we performed additional analyses including TTV as a covariate.

Covariation Between Brain Volumes and FMRP Level or IQ

Based on previous studies in older individuals with FXS, we hypothesized that caudate volumes would show a significant negative correlation with the FMRP level[4] (note that a lower FMRP level is thought to be correlated with greater severity of FXS). We therefore correlated caudate GMV, which showed significant differences between FXS and controls in VBM and caudate volumes from manual measurements, with FMRP level in the FXS group. Regression analysis with IQ (Mullen Scales of Early Learning composite SS) as the dependent measure was also performed for the TD, FXS, and DD groups separately. A statistical threshold with a joint-expected probability[20] of $P = .01$ for height and extent was used.

Multivariate Pattern Classification Analyses

The final analysis was designed to identify regions where spatially distributed GMV patterns carried information specific to FXS using a machine learning approach, support vector machine analysis.[21-24] First, we resampled unsmoothed GMV maps to 4×4-mm voxels within the custom GM template and computed an n-dimensional GMV vector $v_{f,1\ldots n}$ for each subject with FXS (f) and $v_{c,1\ldots n}$ for each control subject (c) except for 1 subject (leave-one-out cross-validation). These represent spatial GMV patterns for n voxels. This was transformed to normalized GMV vectors $V_{f,1\ldots n}$ and $V_{c,1\ldots n}$. Next, we performed principal component analysis to reduce the number of features and used the number of eigenvectors that accounted for variance above 80%, which gave $F_{f,1\ldots N}$ and $F_{c,1\ldots N}$ for N (3) features. We assigned the vectors for n−1 subjects as a training data set that was used to train a linear support vector pattern classifier (with a fixed regularization parameter $C = 1$) to correctly identify GMV patterns of the n^{th} subject, which was repeated n times. Prediction accuracy, sensitivity, specificity, and positive predictive values were calculated. Weight vectors were transformed back to voxel space as described by Mourão-Miranda et al.[24] We repeated the analyses to classify FXS from TD and FXS from DD separately as well as to classify DD from TD. Because there were only 18 DD subjects (vs 51 subjects with FXS), we ensured that the low classification accuracy of DD from TD was not due to small sample size by randomly selecting 18 subjects with FXS and classifying these subjects with FXS from TD subjects (which yielded high classification accuracy). Classification accuracies of FXS from TD and DD from TD were statistically compared using permutation analyses.

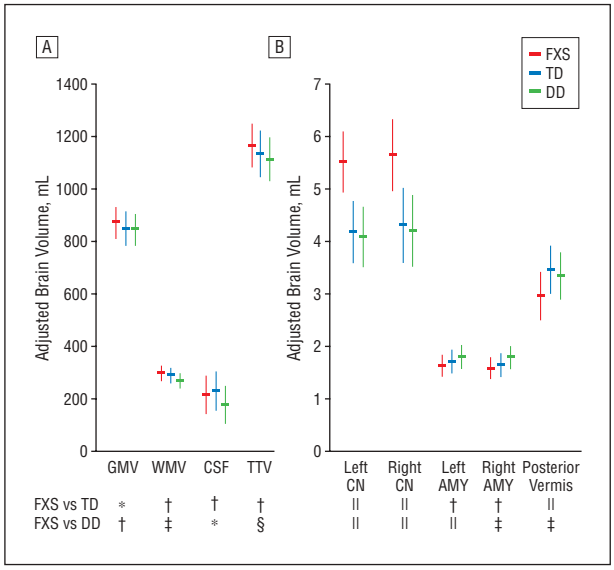

Figure 3. Adjusted brain volumes for each group. A, Total gray matter volume (GMV), total white matter volume (WMV), total cerebrospinal fluid volume (CSF), and total tissue volume (TTV) (GMV + WMV) are adjusted for age and scan site. B, Left and right caudate nuclei (CN) volumes, left and right amygdala (AMY) volumes, and posterior vermis volume are adjusted for age, scan site, and TTV. Error bars indicate SD; FXS, fragile X syndrome; TD, typically developing; and DD, developmentally delayed. *$P < .10$. †$P \geq .10$. ‡$P < .01$. §$P < .05$. ||$P < .001$.

We also performed identical support vector machine analyses but used different methods to define features. The aforementioned method including all of the GM 4×4-mm voxels is referred to as the voxelwise feature selection method. To compare with this method, we coregistered all of the 116 brain regions in the Automated Talairach Atlas Label (http://www.cyceron.fr/freeware/) to subjects' unsmoothed normalized images, extracted GMV from all of the regions, and repeated the analysis (regionwise). Classification accuracies of the voxelwise and regionwise methods were statistically compared using permutation analyses.

Because caudate volumes on their own were relatively good classifiers, we also repeated the voxelwise analysis including all of the GM voxels but excluding voxels in the caudate (voxelwise excluding caudate). The caudate was defined using the Automated Talairach Atlas Label. These methods were also performed in a leave-one-out fashion.

Discriminating volumes (weight vectors transformed back into brain space) were presented in 2 ways. First, we showed weights of all of the voxels without any thresholding. We also showed voxels that exceeded a specified statistical threshold using permutation analysis (random assignment of classes 2000 times; $P = .05$, weight = ±0.0054).

RESULTS

Univariate whole-brain voxelwise analysis showed significantly greater GMV in FXS compared with TD and DD controls in specific regions that included the bilateral caudate, occipital cortex including fusiform gyrus, hypothalamus, and thalamus. In contrast, FXS showed significantly reduced GMV in the superior temporal gyrus, hippocampus, insula, orbitofrontal cortex, and medial pre-

Table 4. Brain, Caudate, Amygdala, and Cerebellar Vermis Volumes

Brain Volume	Adjusted	Volume, Mean (SD), mL			*P* Value[a]			
		FXS (n=51)	TD (n=32)	DD (n=18)	ANOVA	FXS vs TD	FXS vs DD	TD vs DD
Gray matter	Age, site	872.00 (62.00)	847.25 (63.80)	844.87 (61.30)	.13	NA	NA	NA
White matter	Age, site	294.66 (30.30)	287.24 (31.20)	267.31 (30.00)	.005	.30	.001	.03
Cerebrospinal fluid	Age, site	212.75 (71.10)	228.59 (73.20)	175.32 (70.30)	.05	.35	.05	.01
Total tissue[b]	Age, site	1166.65 (85.00)	1134.50 (87.50)	1112.18 (84.00)	.04	.11	.02	.38
Left caudate	Age, site, TTV	5.50 (0.58)	4.18 (0.59)	4.08 (0.58)	<.001	<.001	<.001	.56 (.34)
Right caudate	Age, site, TTV	5.63 (0.69)	4.30 (0.71)	4.19 (0.69)	<.001	<.001	<.001	.58 (.37)
Left amygdala[c]	Age, site, TTV	1.62 (0.21)	1.70 (0.23)	1.79 (0.22)	.002 (.07)	.20 (.73)	<.001 (.02)	.02 (.08)
Right amygdala[c]	Age, site, TTV	1.57 (0.21)	1.63 (0.22)	1.78 (0.21)	.02 (.35)	.14 (.60)	.007 (.15)	.17 (.39)
Anterior vermis	Age, site, TTV	4.84 (0.55)	4.81 (0.56)	4.76 (0.54)	.86 (.49)	NA	NA	NA
Middle vermis	Age, site, TTV	2.84 (0.51)	2.98 (0.52)	2.99 (0.51)	.42 (.62)	NA	NA	NA
Posterior vermis	Age, site, TTV	2.95 (0.46)	3.45 (0.46)	3.34 (0.45)	<.001	<.001	.02 (.003)	.28

Abbreviations: ANOVA, analysis of variance; DD, developmentally delayed; FXS, fragile X syndrome; NA, not applicable; TD, typically developing; TTV, total tissue volume.

[a] Results adjusting for age and site are noted in parentheses when different from results adjusting for age, site, and TTV.

[b] Total tissue volume is the sum of the gray matter volume plus the white matter volume.

[c] The sample sizes were 50 for FXS, 28 for TD, and 16 for DD.

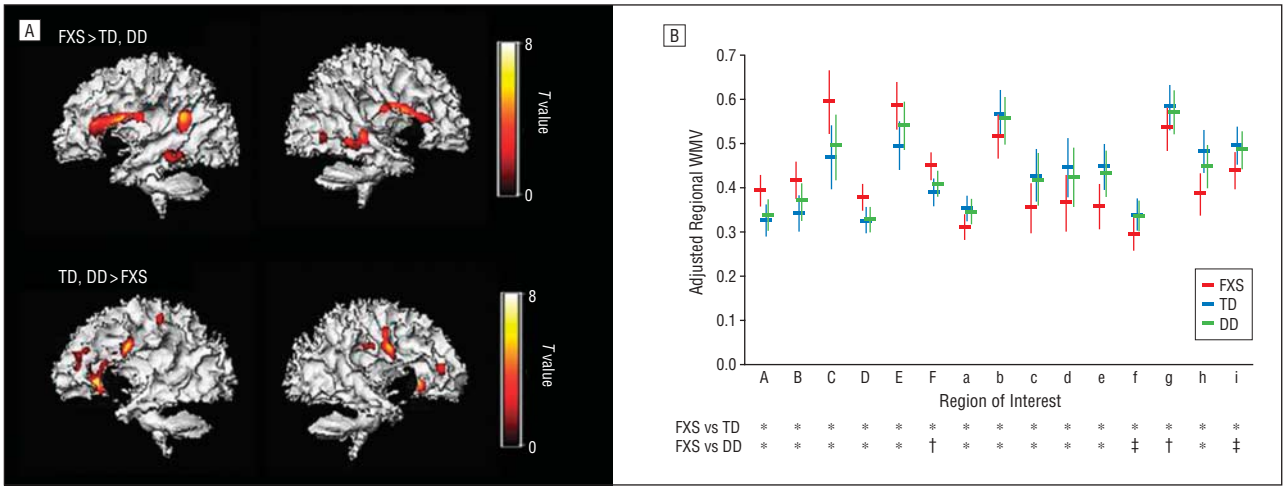

Figure 4. Regional white matter volume (WMV) differences between groups. A, White matter regions that show significantly greater and less volumes in fragile X syndrome (FXS) compared with typically developing (TD) and developmentally delayed (DD) groups. $P=.05$, familywise-error corrected, extent threshold=200. Age, scan site, and total WMV were entered as nuisance variables. Statistical maps are overlaid on a representative image of the segmented white matter of a single subject with FXS (top) and a TD subject (bottom). B, Brain volumes adjusted for age, scan site, and total WMV from regions in part A are extracted and plotted to ensure that one of the control groups (TD or DD) is not driving the effect. Letters on the x-axis correspond to region of interest labels in Table 3. Error bars indicate SD. *$P<.001$. †$P<.01$. ‡$P<.05$.

frontal cortices (PFCs) compared with TD and DD (**Figure 1** and Table 2). Probabilistic maps from permutation analysis show the highly reliable nature of the results (**Figure 2**). Volumetric measures were consistent with the whole-brain results (**Figure 3** and **Table 4**). Results from WM regions with significantly different WMV between FXS and controls in the prefrontal and temporal regions are shown in **Figure 4** and Table 3. Within FXS, FMRP levels were significantly (negatively) correlated with bilateral caudate volumes identified from both VBM and volumetric analyses ($P<.05$).

Next, covariation between cognitive functioning (IQ) and morphometric patterns was examined. In TD, IQ showed significant positive correlations with cerebellar hemispheres (left>right), vermis, and fusiform gyrus GMV and negative correlations with right dorsolateral PFC, bilateral medial PFC, and orbitofrontal cortex GMV and medial prefrontal WMV (**Figure 5**). In DD, there were significant positive correlations between IQ and GMV in bilateral parietotemporal regions and negative correlations between IQ and WMV in a medial prefrontal region adjacent to that found in TD. In contrast, significant (negative) brain-IQ associations were observed in FXS in the left parietotemporal region, similar to DD, but not in other regions.

We adopted machine learning algorithms to examine whether whole-brain voxelwise spatial patterns of GMV could discriminate between groups. Although the spatial resolution of human neuroimaging is limited, hence leaving most studies to examine extended regions of the brain, it has recently been shown that MRI can be used to study fine-grained neural representations even when

they are encoded at a finer scale than the resolution of the measurement grid.[22] Using a leave-one-out linear support vector machine approach, FXS was discriminated from controls with 92.9% classification accuracy (**Figure 6**A). Classification accuracy between FXS and TD was significantly better than between DD and TD even when matched for the small sample size of DD subjects ($P < .001$) (Figure 6A). Comparisons across support vector machine methods showed the importance of voxelwise spatial information in classification accuracy rather than using more coarse region-based measures (116 anatomical labels, http://www.cyceron.fr/freeware/) of GMV ($P < .001$) (Figure 6A). This was presumably due to the mixture of voxels that showed both increased and decreased GMV in a given region (eg, medial vs lateral amygdala, hippocampus, and posterior vermis) (Figure 6B). Finally, because an enlarged caudate volume is the most characteristic morphometric feature in FXS, we repeated the classification analysis excluding caudate voxels and still obtained high classification accuracy (88.9%) (Figure 6A).

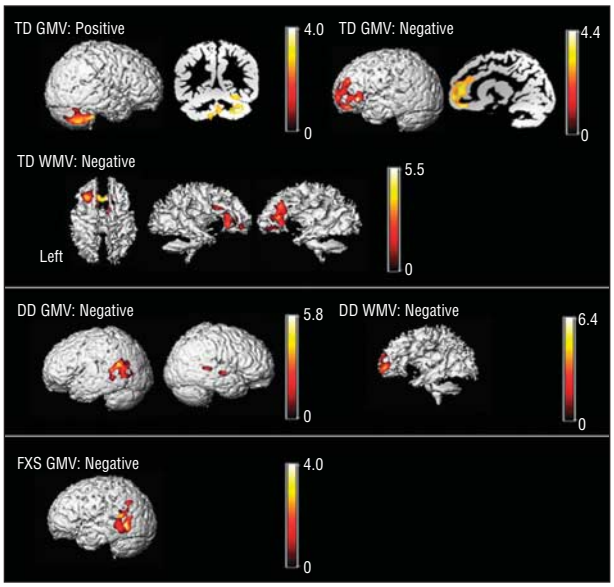

Figure 5. Covariation of regional brain volumes and IQ. Gray matter and white matter regions that show significant correlation with IQ (Mullen Scales of Early Learning composite standard score) in typically developing (TD) and developmentally delayed (DD) groups (the fragile X syndrome [FXS] group showed no significant correlation). $P = .01$, corrected. Volumes are adjusted for age, scan site, total gray matter volume (GMV) (for gray matter regions), and white matter volume (WMV) (for white matter regions). Statistical maps are overlaid on a representative image of the segmented gray matter (for gray matter regions) or white matter (for white matter regions) of a single TD subject (for correlations in the TD group) or DD subject (for correlations in the DD group). Scaling bars represent *T* values. The left side shows the left hemisphere except when noted.

COMMENT

In this study, voxelwise structural brain profiles obtained from healthy children aged 1 to 3 years were characterized and compared with profiles obtained from children with a specific neurodevelopmental disorder, FXS, and an idiopathic DD group. Findings of increased caudate, fusiform gyrus, and thalamus GMV as well as reduced superior temporal gyrus, hippocampus, and orbitofrontal cortex GMV from the univariate voxelwise analysis partially replicate results from studies of older individuals with FXS.[4-7] Associations between larger caudate volumes and reduced levels of FMRP (generally reflecting lower functioning in FXS) also replicate findings in studies of older individuals with FXS.[5,8] Further, WM abnormalities within the medial prefrontal region are in line with a diffusion tensor imaging study in female adolescents with FXS[25] and support the finding of executive function deficits in FXS. The detection of abnormal morphology of these regions in children as young as 18 months suggests that early genetic influences significantly influence selected components of neurodevelopment during the prenatal period or early infancy in FXS. Similar patterns of neuroanatomical differences observed between FXS and TD and between FXS and DD also point to the specificity of early neurodevelopmental abnormalities resulting from the *FMR1* full mutation as opposed to the nonspecific effects of DD. Unlike previous observations in older subjects,[5] abnormal size in regions such as the amygdala was not observed in FXS with voxel-based or volumetric analyses. However, pattern classification analyses indicated that a mixture of vox-

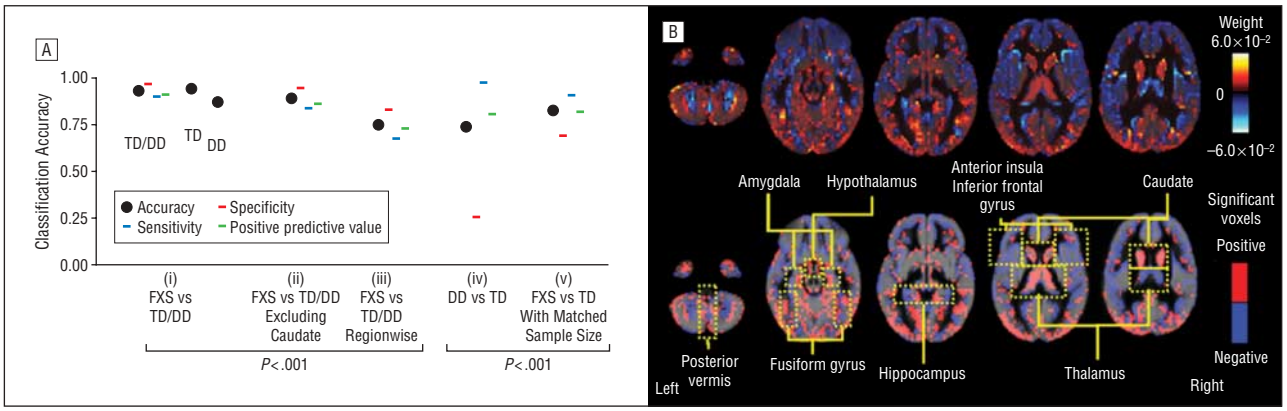

Figure 6. Pattern classification results. A, Classification accuracy. Support vector machine analysis results classifying fragile X syndrome (FXS) and controls using all gray matter voxels (i), all gray matter voxels except caudate voxels (ii), and 116 brain regions (iii). The support vector machine analysis results classifying developmentally delayed (DD) from typically developing (TD) using all GM voxels (iv) and classifying FXS from TD in a subset of randomly selected subjects with FXS (n=18) to match the sample size of DD (v) are shown. B, Whole-brain representation of pattern classification results from FXS vs TD or DD using all gray matter voxels. Axial brain images of weight vectors from leave-one-out support vector machine analysis for all voxels (top) and spatial patterns of the most significant voxels when thresholded at $P = .05$ (according to 2000 permutations) (bottom) are shown.

els exists, with both increased and decreased volumes in a medial and lateral fashion within such regions (note similar patterns in the hippocampus and posterior vermis in Figure 6B). The classification results indicate the complexity of genetic influences on brain morphology rather than a model in which genetic factors uniformly affect a given brain region. Replication of these results in longitudinal studies is warranted. Future research can benefit from the inclusion of larger samples of TD and DD controls.

On the other hand, several regions that were not identified as morphologically aberrant in previous studies of older individuals with FXS were observed here: enlarged hypothalamus and smaller insula, medial PFC, and lateral PFC. The hypothalamus finding is of particular interest in light of hypothalamic-pituitary-adrenal dysfunction and abnormal stress responses found in both children with FXS[26] and the animal model of this disorder.[27] Abnormal insula and medial PFC volumes in FXS are consistent with observations of aberrant insula and medial PFC activation during gaze processing,[28] hyperarousal,[29] and the social and cognitive features shared with autism.[30] These findings indicate that the seeds of social cognitive dysfunction observed in FXS are likely to arise directly from neurodevelopmental effects of the mutation later interacting with common environmental influences. Further, it is possible that abnormality of the lateral PFC, in concert with aberrant caudate morphology, may be responsible for the known executive function (response inhibition) deficit, hyperactivity, and frontostriatal dysfunction in FXS.[4,31,32] Lastly, it is possible that some of the abnormalities observed in very young but not older individuals with FXS "normalize" over the course of development, at least in terms of volumes. Indeed, dendritic spine abnormalities in mouse models of FXS have been shown to diminish in certain brain regions during development.[33] The exact mechanisms, however, remain to be elucidated.

Another finding of note is the association between regional brain volumes and IQ. The TD group showed a negative association between IQ and prefrontal GMV. This finding is consistent with what has been shown previously in healthy children aged 3.8 to 8.4 years.[2] We add to this and demonstrate that similar results are observed in younger TD children. We also present novel findings suggesting associations between anatomy and IQ for fusiform gyrus and cerebellar GM (TD group) and medial prefrontal WM in both TD and DD (but not in FXS). The negative association with the parietotemporal region appeared nonspecific and was found in both DD and FXS.

Finally, we illustrate that fine spatial patterns of GMV accurately predict whether a child has FXS. Similar analytical strategies as applied to functional neuroimaging data have been shown to be a powerful tool in decoding mental states within individuals where traditional massive univariate general linear models fail.[22] Here we show their usefulness in classifying disease using structural neuroimaging data. These findings may inform future studies predicting cognitive outcome in FXS as well as research focused on children with other neurodevelopmental syndromes. Further, these findings have implications for understanding the genetic control of healthy brain development.

Submitted for Publication: January 12, 2008; final revision received March 11, 2008; accepted April 16, 2008.
Correspondence: Fumiko Hoeft, MD, PhD, Department of Psychiatry and Behavioral Sciences, Stanford University School of Medicine, 401 Quarry Rd, Stanford, CA 94305-5795 (fumiko@stanford.edu).
Author Contributions: Dr Hoeft had full access to all of the data in the study and takes responsibility for the integrity of the data and the accuracy of the data analysis.
Financial Disclosure: None reported.
Funding/Support: This study was funded by grants MH64708-05 (Drs Piven and Reiss), MH61696 (Dr Piven), and HD03110-36 (Dr Piven) from the National Institutes of Health and by the Child Health Research Program from the Stanford University School of Medicine (Dr Hoeft).
Additional Contributions: We sincerely thank all of the families who made this study possible. Chad Chappell, MA, Nancy Garrett, BA, Michael Graves, MChe, Cindy Hagan, BA, Cindy Johnston, MS, Arianna Martin, BA, Robin Morris, BA, Judy Morrow, PhD, Matthew Mosconi, PhD, Rachel Smith, BA, Cristiana Vattuone, BA, Christa Watson, BA, and Anh Weber, PhD, were involved in data collection.

REFERENCES

1. Toga AW, Thompson PM, Sowell ER. Mapping brain maturation. *Trends Neurosci.* 2006;29(3):148-159.
2. Shaw P, Greenstein D, Lerch J, Clasen L, Lenroot R, Gogtay N, Evans A, Rapoport J, Giedd J. Intellectual ability and cortical development in children and adolescents. *Nature.* 2006;440(7084):676-679.
3. Greenough WT, Klintsova AY, Irwin SA, Galvez R, Bates KE, Weiler IJ. Synaptic regulation of protein synthesis and the fragile X protein. *Proc Natl Acad Sci U S A.* 2001;98(13):7101-7106.
4. Reiss AL, Dant CC. The behavioral neurogenetics of fragile X syndrome: analyzing gene-brain-behavior relationships in child developmental psychopathologies. *Dev Psychopathol.* 2003;15(4):927-968.
5. Gothelf D, Furfaro JA, Hoeft F, Eckert MA, Hall SS, O'Hara R, Erba HW, Ringel J, Hayashi KM, Patnaik S, Golianu B, Kraemer HC, Thompson PM, Piven J, Reiss AL. Neuroanatomy of fragile X syndrome is associated with aberrant behavior and the fragile X mental retardation protein (FMRP). *Ann Neurol.* 2008;63(1):40-51.
6. Kates WR, Folley BS, Lanham DC, Capone GT, Kaufmann WE. Cerebral growth in Fragile X syndrome: review and comparison with Down syndrome. *Microsc Res Tech.* 2002;57(3):159-167.
7. Lee AD, Leow AD, Lu A, Reiss AL, Hall S, Chiang MC, Toga AW, Thompson PM. 3D pattern of brain abnormalities in Fragile X syndrome visualized using tensor-based morphometry. *Neuroimage.* 2007;34(3):924-938.
8. Reiss AL, Abrams MT, Greenlaw R, Freund L, Denckla MB. Neurodevelopmental effects of the FMR-1 full mutation in humans. *Nat Med.* 1995;1(2):159-167.
9. Mullen EM. *Mullen Scales of Early Learning AGS Edition.* Circle Pines, MN: American Guidance Service Inc; 1995.
10. Oberlé I, Rousseau F, Heitz D, Kretz C, Devys D, Hanauer A, Boué J, Bertheas MF, Mandel JL. Instability of a 550-base pair DNA segment and abnormal methylation in fragile X syndrome. *Science.* 1991;252(5010):1097-1102.
11. Willemsen R, Mohkamsing S, de Vries B, Devys D, van den Ouweland A, Mandel JL, Galjaard H, Oostra B. Rapid antibody test for fragile X syndrome. *Lancet.* 1995;345(8958):1147-1148.
12. Sparrow SS, Balla DA, Cicche HV. *Vineland Adaptive Behavior Scales–Interview Edition Survey Form Manual.* Circle Pines, MN: American Guidance Service Inc; 1984.
13. Achenbach TM, Ruffle TM. The Child Behavior Checklist and related forms for assessing behavioral/emotional problems and competencies. *Pediatr Rev.* 2000;21(8):265-271.

14. Bodfish JW, Crawford TW, Powell SB, Parker DE, Golden RN, Lewis MH. Compulsions in adults with mental retardation: prevalence, phenomenology, and comorbidity with stereotypy and self-injury. *Am J Ment Retard*. 1995;100(2):183-192.
15. Bodfish JW, Symons F, Lewis MH. *The Repetitive Behavior Scales*. Morganton, NC: Western Carolina Center Research Reports; 1999.
16. Xia Y, Bettinger K, Shen L, Reiss AL. Automatic segmentation of the caudate nucleus from human brain MR images. *IEEE Trans Med Imaging*. 2007;26(4):509-517.
17. Schumann CM, Hamstra J, Goodlin-Jones BL, Lotspeich LJ, Kwon H, Buonocore MH, Lammers CR, Reiss AL, Amaral DG. The amygdala is enlarged in children but not adolescents with autism; the hippocampus is enlarged at all ages. *J Neurosci*. 2004;24(28):6392-6401.
18. Henkelman RM. Measurement of signal intensities in the presence of noise in MR images. *Med Phys*. 1985;12(2):232-233.
19. Talairach J, Tournoux P. *Co-planar Stereotaxic Atlas of the Human Brain*. New York, NY: Thieme; 1988.
20. Poline JB, Worsley KJ, Evans AC, Friston KJ. Combining spatial extent and peak intensity to test for activations in functional imaging. *Neuroimage*. 1997;5(2):83-96.
21. Burges CJC. A tutorial on support vector machines for pattern recognition. *Data Min Knowl Discov*. 1998;2(2):121-167.
22. Haynes JD, Rees G. Decoding mental states from brain activity in humans. *Nat Rev Neurosci*. 2006;7(7):523-534.
23. Haynes JD, Sakai K, Rees G, Gilbert S, Frith C, Passingham RE. Reading hidden intentions in the human brain. *Curr Biol*. 2007;17(4):323-328.
24. Mourão-Miranda J, Reynaud E, McGlone F, Calvert G, Brammer M. The impact of temporal compression and space selection on SVM analysis of single-subject and multi-subject fMRI data. *Neuroimage*. 2006;33(4):1055-1065.
25. Barnea-Goraly N, Eliez S, Hedeus M, Menon V, White CD, Moseley M, Reiss AL. White matter tract alterations in fragile X syndrome: preliminary evidence from diffusion tensor imaging. *Am J Med Genet B Neuropsychiatr Genet*. 2003;118B(1):81-88.
26. Hessl D, Rivera SM, Reiss AL. The neuroanatomy and neuroendocrinology of fragile X syndrome. *Ment Retard Dev Disabil Res Rev*. 2004;10(1):17-24.
27. Lauterborn JC. Stress induced changes in cortical and hypothalamic c-fos expression are altered in fragile X mutant mice. *Brain Res Mol Brain Res*. 2004;131(1-2):101-109.
28. Watson C, Hoeft F, Garrett AS, Hall SS, Reiss AL. Aberrant brain activation during gaze processing in males with fragile X syndrome. *Arch Gen Psychiatry*. In press.
29. Miller LJ, McIntosh DN, McGrath J, Shyu V, Lampe M, Taylor AK, Tassone F, Neitzel K, Stackhouse T, Hagerman RJ. Electrodermal responses to sensory stimuli in individuals with fragile X syndrome: a preliminary report. *Am J Med Genet*. 1999;83(4):268-279.
30. Belmonte MK, Bourgeron T. Fragile X syndrome and autism at the intersection of genetic and neural networks. *Nat Neurosci*. 2006;9(10):1221-1225.
31. Hoeft F, Hernandez A, Parthasarathy S, Watson CL, Hall SS, Reiss AL. Fronto-striatal dysfunction and potential compensatory mechanisms in male adolescents with fragile X syndrome. *Hum Brain Mapp*. 2007;28(6):543-554.
32. Menon V, Leroux J, White CD, Reiss AL. Frontostriatal deficits in fragile X syndrome: relation to *FMR1* gene expression. *Proc Natl Acad Sci U S A*. 2004;101(10):3615-3620.
33. Bagni C, Greenough WT. From mRNP trafficking to spine dysmorphogenesis: the roots of fragile X syndrome. *Nat Rev Neurosci*. 2005;6(5):376-387.